ADVANCES IN ATMOSPHERIC SCIENCES, VOL. 34, FEBRUARY 2017, 144–156

• **Original Paper** •

Responses of the East Asian Jet Stream to the North Pacific Subtropical Front in Spring

Leying ZHANG[1,2], Haiming XU[*1,2], Ning SHI[1,2], and Jiechun DENG[1,2]

[1]*Collaborative Innovation Center on Forecast and Evaluation of Meteorological Disasters/Key Laboratory of Meteorological Disaster, Ministry of Education/Joint International Research Laboratory of Climate and Environment Change, Nanjing University of Information Science and Technology, Nanjing* 210044*, China*

[2]*College of Atmospheric Science, Nanjing University of Information Science and Technology, Nanjing* 210044*, China*

(Received 28 January 2016; revised 26 May 2016; accepted 3 June 2016)

ABSTRACT

This study concerns atmospheric responses to the North Pacific subtropical front (NPSTF) in boreal spring over the period 1982–2014. Statistical results show that a strong NPSTF in spring can significantly enhance the East Asian jet stream (EAJS). Both transient eddy activity and the atmospheric heat source play important roles in this process. The enhanced atmospheric temperature gradient due to a strong NPSTF increases atmospheric baroclinicity, resulting in an intensification of transient eddy and convection activities. On the one hand, the enhanced transient eddy activities can excite an anomalous cyclonic circulation with a quasi-baraotropical structure in the troposphere to the north of the NPSTF. Accordingly, the related westerly wind anomalies around 30°N can intensify the component of the EAJS over the Northeast Pacific. On the other hand, an enhanced atmospheric heat source over the NPSTF, which is related to increased rainfall, acts to excite an anomalous cyclonic circulation system in the troposphere to the northwest of the NPSTF, which can explain the enhanced component of the EAJS over the Northwest Pacific. The two mechanisms may combine to enhance the EAJS.

Key words: North Pacific subtropical front, East Asian jet stream, transient eddy activity, atmospheric heat source

Citation: Zhang, L. Y., H. M. Xu, N. Shi, and J. C. Deng, 2017: Responses of the East Asian jet stream to the North Pacific subtropical front in spring. *Adv. Atmos. Sci.*, **34**(2), 144–156, doi: 10.1007/s00376-016-6026-x.

1. Introduction

Studies using high-resolution satellite observations have revealed that midlatitude SST fronts exert a significant influence on the atmosphere above on both meso and micro timescales (Xie, 2004; Xu et al., 2008, 2010a). These midlatitude SST fronts affect sea surface winds and the atmospheric boundary layer via the SLP adjustment mechanism (Lindzen and Nigam, 1987; Small et al., 2003) and vertical mixing mechanism (Hayes et al., 1989; Wallace et al., 1989).

In addition to the atmospheric responses in the atmospheric boundary layer, midlatitude SST fronts also have marked impacts on the whole troposphere (Brayshaw et al., 2008; Nakamura and Miyama, 2014), through their effects on baroclinicity (Nakamura and Yamane, 2010; O'Reilly and Czaja, 2015) and convective activities (Kobashi et al., 2008). Sampe et al. (2010) found that an SST front over the midlatitudes is conducive to the formation of the jet stream and storm tracks, and its displacement can shift the jet stream and storm tracks in the same direction (Ogawa et al., 2012; Nakamura and Miyama, 2014). Additionally, an SST front over the midlatitudes corresponds to a convective rainfall maximum (Minobe et al., 2008) and frequent lightning activities (Tokinaga et al., 2009)—a finding confirmed by numerical simulations (Kuwano-Yoshida et al., 2010; Xu et al., 2011).

Many studies have demonstrated the significant influences of SST fronts on the atmosphere over the western North Pacific, especially over the East China Sea (Xie et al., 2002; Xu et al., 2010b; Xu and Xu, 2015), the Kuroshio extension, and the Oyashio extension (Tanimoto et al., 2009; Kwon et al., 2010). In addition to these midlatitude SST fronts mentioned above, a maximum SST gradient exists over the Northwest Pacific around 25°N in spring; namely, the North Pacific subtropical front (NPSTF; Fig. 1). Although many efforts have been made to elucidate the formation mechanism of the NPSTF in terms of intrinsic ocean dynamics (Yoshida and Kidokoro, 1967a, 1967b; Roden, 1975; Kubokawa, 1995, 1997, 1999; Kobashi and Kubokawa, 2012), little is known about its synoptic and climatic impacts on the atmosphere.

Xie (2004) suggested that the air–sea coupling effect is robust around the SST front over the world's oceans. Since the NPSTF is located farther south and has a higher SST

* Corresponding author: Haiming XU
Email: hxu@nuist.edu.cn

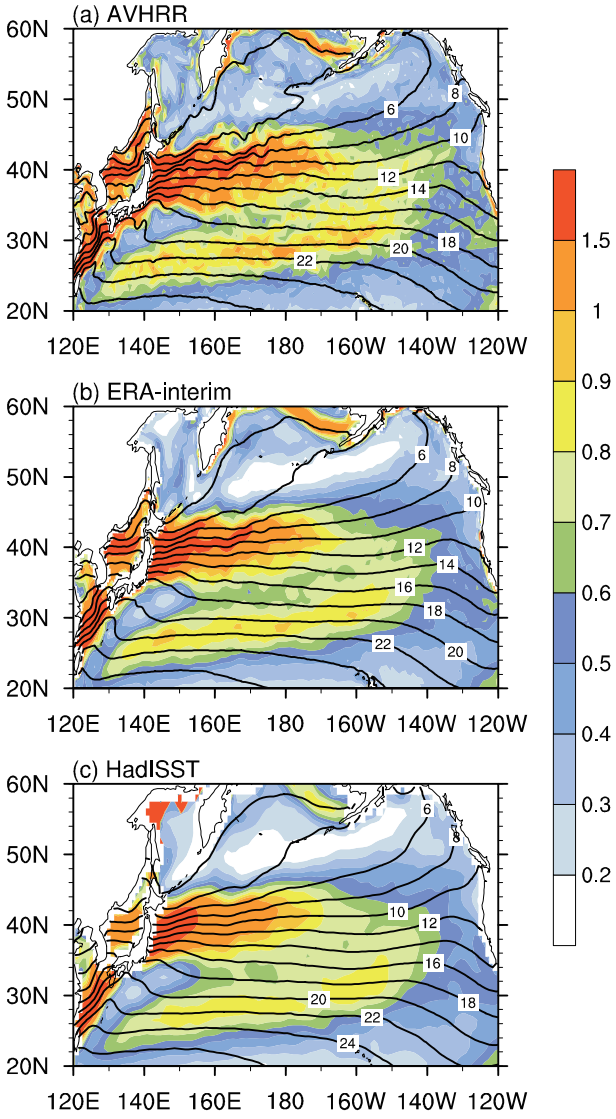

Fig. 1. Climatological spring SST (contours; units: °C) and SST gradient [color shading; units: °C (100 km)$^{-1}$] during 1982–2014: (a) AVHRR; (b) ERA-Interim; (c) HadISST. The amplitude of the SST gradient is measured by $\sqrt{(\partial \mathrm{SST}/\partial x)^2 + (\partial \mathrm{SST}/\partial y)^2}$.

with respect to the midlatitude SST front, it is likely that the NPSTF can significantly affect large-scale atmospheric circulation by changing atmospheric baroclinicity and convective activities. In fact, Kobashi et al. (2008) demonstrated that the synoptic low above the SST front can be enhanced during April–May, due to increased atmospheric baroclinicity and condensation latent heat release caused by the NPSTF. However, little is known about the impacts of the NPSTF on the free atmosphere on the interannual timescale.

As is well known, the East Asian jet stream (EAJS) is an important circulation system over the North Pacific. The variability of the intensity and location of the EAJS also exerts a significant influence on the weather and climate over East Asia (Liang and Wang, 1998; Zhang et al., 2008; Lu et al., 2013). Ye et al. (1958) suggested that the seasonal variability of the EAJS produces two significant abrupt changes in the atmospheric circulation over East Asia during June and December, leading to subsequent anomalous weather and climate. Xie et al. (2015) found that the subtropical westerly jet stream exhibits a significant zonal pattern associated with its seasonal evolution, which affects both large-scale atmospheric circulation and precipitation over East Asia and the North Pacific. Moreover, numerous studies have shown that the EAJS can act as a waveguide and transmit the signals to remote regions, inducing anomalous climatic responses over these regions, e.g., the Arctic Oscillation (Gong and Ho, 2003), the North Atlantic Oscillation (Watanabe, 2004) and the Eurasian teleconnection (Wang and Zhang, 2015).

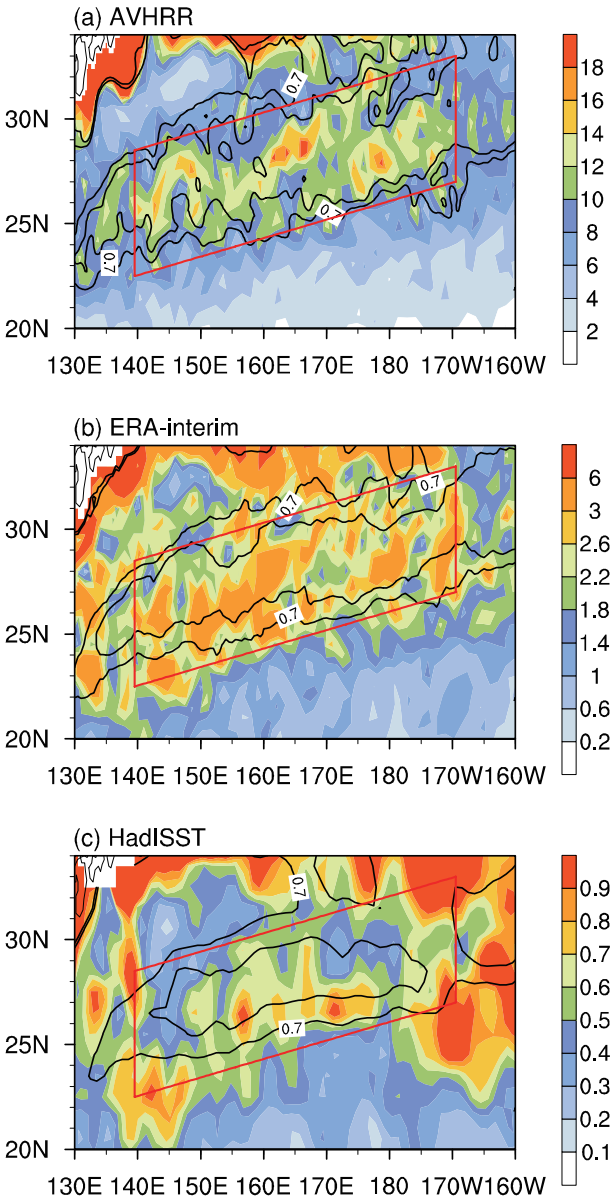

Fig. 2. Climatological spring SST gradient [contours; only 0.7 and 0.8°C (100 km)$^{-1}$ shown] and its variance (color shading). The red box indicates the key area of the NPSTF.

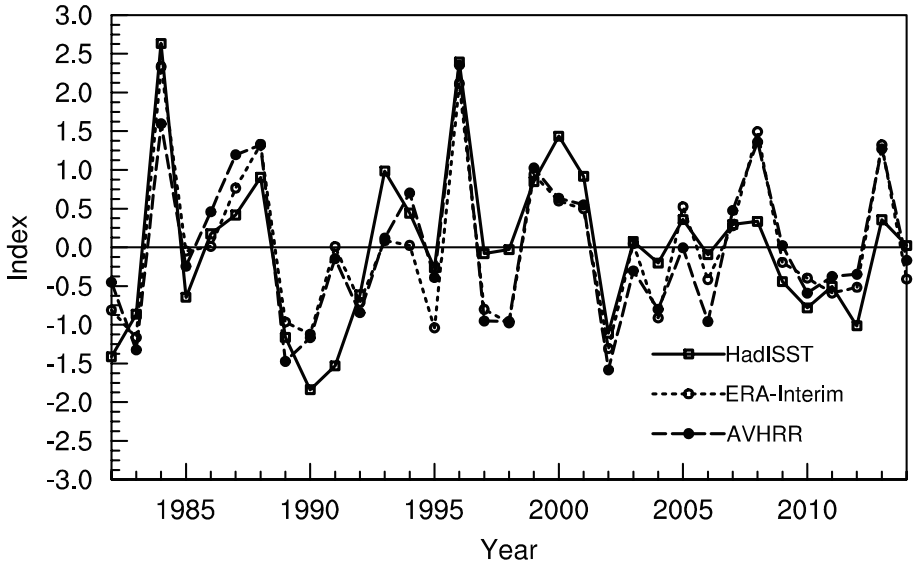

Fig. 3. The NPSTF index for the period 1982–2014 using three datasets.

Therefore, exploring the linkage between the NPSTF and the EAJS should improve our understanding of the interactions among the circulation systems over East Asia and the western Pacific. Here, we focus on the responses of the EAJS to the intensity of the NPSTF during boreal spring, when the NPSTF reaches its maximum intensity.

The rest of the paper is organized as follows: We introduce the reanalysis datasets and methods used in this study in section 2. The statistical relationship between the intensity of the NPSTF and the EAJS is presented in section 3. We discuss the possible processes by which the NPSTF affects the EAJS in section 4. Numerical experiments are used to confirm the relationship between the NPSTF and the EAJS in section 5. A summary and discussion are given in section 6.

2. Data and methods

2.1. *Data*

We use three SST datasets to identify the spatial and temporal characteristics of the NPSTF: HadISST, which provides monthly-mean SST at a resolution of $1^\circ \times 1^\circ$ (Rayner et al., 2003); monthly-mean ERA-Interim SST at a resolution of $0.5^\circ \times 0.5^\circ$ (Dee et al., 2011); and daily-mean AVHRR SST, from the NCDC of NOAA, at a resolution of $0.25^\circ \times 0.25^\circ$ (Reynolds and Chelton, 2010). The NPSTF index is defined as the normalized anomalies of the amplitude of SST gradient over its maximum region.

The atmospheric data used in this study, expect for precipitation, are the 6-hourly ERA-Interim data, at a horizontal resolution of $1.5^\circ \times 1.5^\circ$, for wind, air temperature, geopotential height, and SLP. The 6-hourly fields are averaged to obtain daily-mean fields. In order to evaluate the high-frequency transient eddy feedback forcing, an 8-day high-pass filter is applied to these daily fields. Precipitation data are the monthly-mean data of CMAP, at a resolution of $2.5^\circ \times 2.5^\circ$. For consistency, all variables used in this study cover the period from January 1982 to December 2014.

Since the NPSTF index has a significant increasing tendency [Fig. S1 in electronic supplementary material (ESM)], the long-term linear trends are removed for all variables before further calculations. In order to obtain the interannual variability, we also perform Fourier analysis to remove the first three waves, which are usually related to interdecadal variability (Awan and Bae, 2016).

2.2. *Atmospheric baroclinicity index*

Baroclinicity is generally measured by a combination of static stability and horizontal temperature gradient. The latter is equivalent to vertical shear of the horizontal wind according to the thermal wind balance (Charney, 1947; Eady, 1949).

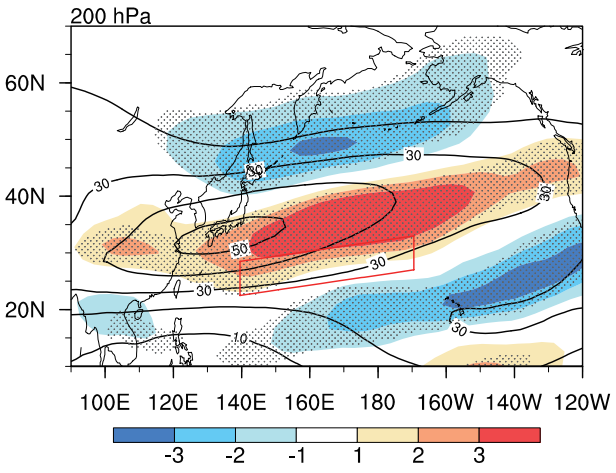

Fig. 4. Regression coefficients of 200 hPa wind speed (color shading; units: m s^{-1}) onto the NPSTF index in spring. Contours indicate the climatological spring wind speed. Stippled areas represent statistically significant coefficients exceeding the 95% confidence level.

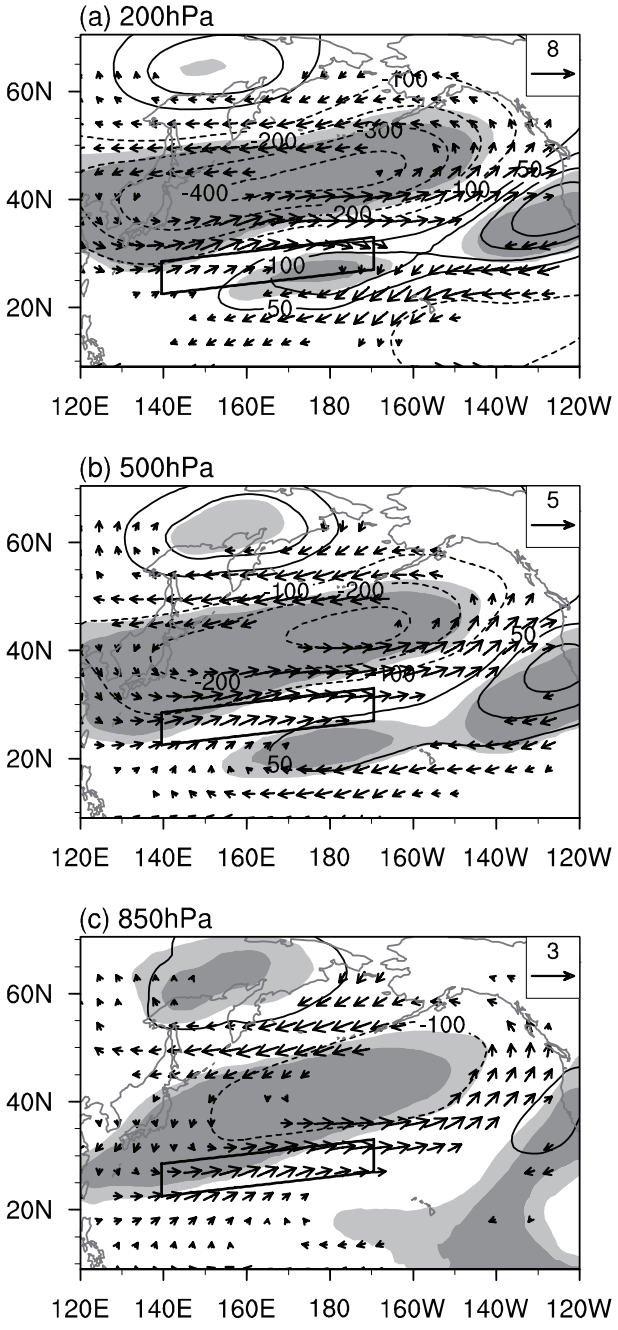

Fig. 5. Regression coefficients of geopotential height (contours; units: $m^2\ s^{-2}$) and horizontal wind (vectors; units: $m\ s^{-1}$) onto the NPSTF index in spring: (a) 200 hPa; (b) 500 hPa; (c) 850 hPa. Contour intervals at the three pressure levels are 50 and 100 $m^2\ s^{-2}$ for positive and negative values, respectively. Light and heavy shading represents statistically significant coefficients exceeding the 95% and 99% confidence levels, respectively. Only the wind component exceeding the 95% confidence level in either direction is shown. The box indicates the key area of the NPSTF.

Lindzen and Farrell (1980) and James (1987) analyzed the baroclinic situation in the background of different air flows and showed that Eady's parameter could successfully estimate the maximum growth rate of baroclinic instability in the troposphere. We use Eady's parameter introduced by Hoskins and Valdes (1990) as the baroclinicity index, shown in Eq. (1):

$$\sigma_{\mathrm{BI}} = 0.31 g N^{-1} T^{-1} |\partial T/\partial y| = 0.31 f |\partial \boldsymbol{V}/\partial z| N^{-1} , \quad (1)$$

where N and f represent the static stability parameter and the Coriolis parameter, respectively; T is air temperature; z is height; and $\boldsymbol{V}$ is horizontal velocity. The larger the baroclinicity index value, the easier it is for synoptic activities to develop (Simmons and Hoskins, 1978). Ignoring the horizontal shears in the lower troposphere and moist processes, this index has been demonstrated to be a good indicator of atmospheric baroclinicity (Nakamura and Sampe, 2002; Nakamura and Yamane, 2010).

2.3. *Atmospheric heat source*

The atmospheric apparent heat source Q_1 consists of the heating due to radiation, the release of latent heat by net condensation, and the vertical convergence of the vertical eddy transport of sensible heat (Yanai et al., 1973; Ding, 1989). The method used here was first introduced in Ding (1989):

$$Q_1 = C_p \left(\frac{p}{p_0}\right)^{R/C_p} \left(\frac{\partial \theta}{\partial t} + \boldsymbol{V}\nabla\theta + \omega \frac{\partial \theta}{\partial p}\right) , \quad (2)$$

where $p_0 = 1000$ hPa, R is the gas constant, C_p is the specific heat capacity of dry air, p is pressure, θ is potential temperature, and ω is pressure vertical velocity. The vertical integration of the atmospheric heat source measures the sensible and latent heat fluxes from the surface into the atmosphere. The positive and negative values indicate the net heat gain and loss of the atmosphere, respectively.

2.4. *High-frequency transient eddy feedback forcing (TEFF)*

TEFF denotes a low-frequency geopotential tendency due to the divergence or convergence of high-frequency transient eddy heat flux and that of vorticity flux. TEFF is vigorous, especially in the middle and high latitudes (Lau and Holopainen, 1984; Lau and Nath, 1991; Shi, 2013).

The feedback forcing can be represented by the geopotential tendency equation (Lau and Holopainen, 1984; Holopainen and Fortelius, 1987):

$$\begin{cases} g\left[\dfrac{1}{f}\nabla^2 + f\dfrac{\partial}{\partial p}\left(\dfrac{1}{\sigma}\dfrac{\partial}{\partial p}\right)\right]\dfrac{\partial Z}{\partial t} = D_{\mathrm{heat}} + D_{\mathrm{vort}} + R \\ D_{\mathrm{heat}} = f\dfrac{\partial}{\partial p}\left(\dfrac{\nabla\cdot\overline{\boldsymbol{V}'\theta'}}{\overline{S}}\right) \\ D_{\mathrm{vort}} = -\nabla\cdot\overline{\boldsymbol{V}'\zeta'} \end{cases} . \quad (3)$$

The boundary conditions at 1000 hPa and 100 hPa are

$$\begin{cases} -\dfrac{gp}{R}\left(\dfrac{p_0}{p}\right)^{R/C_p}\dfrac{\partial}{\partial p}\left(\dfrac{\partial Z}{\partial t}\right)_{\mathrm{heat}} = -\nabla\cdot\overline{\boldsymbol{V}'\theta'} \\ \dfrac{\partial}{\partial p}\left(\dfrac{\partial Z}{\partial t}\right)_{\mathrm{vort}} = 0 \end{cases} , \quad (4)$$

where the prime and overbar represent the variables with high frequency and low frequency, respectively. In Eq. (3), Z is

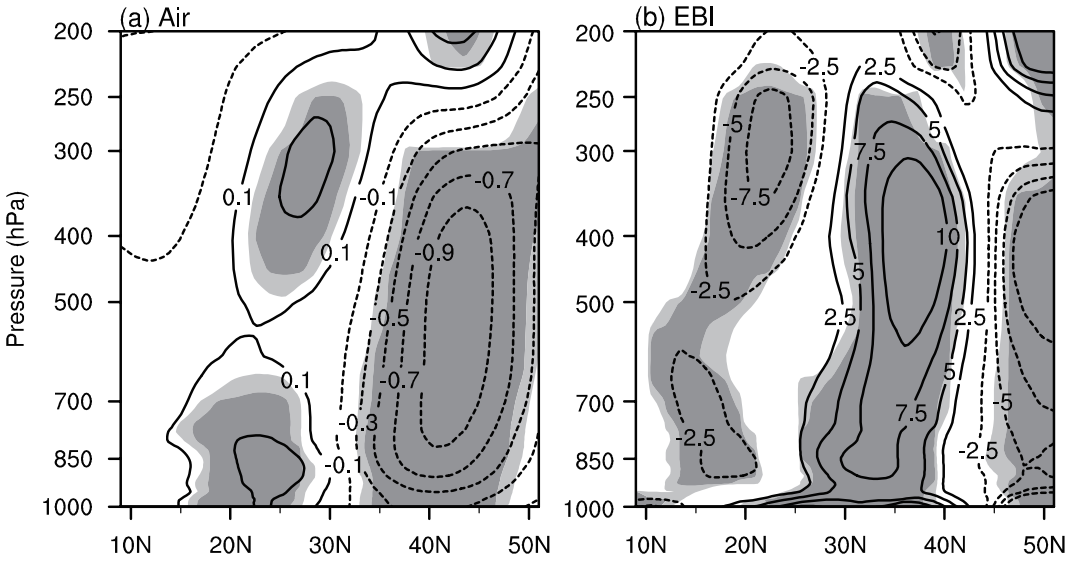

Fig. 6. Latitude–height section of regression coefficients of (a) air temperature (units: °C) and (b) atmospheric baroclinicity index (units: 10^{-2} d^{-1}), zonally averaged over 139.5°E–190.5°W, onto the NPSTF index in spring. Light and heavy shading represents statistically significant coefficients exceeding the 95% and 99% confidence levels, respectively.

height; $\sigma = -(\alpha/\theta)(\partial\theta/\partial p)$ is the static stability parameter, assumed to be a function of pressure only; α is the specific volume, $\boldsymbol{V}'$ is high frequency horizontal velocity; $\overline{S}$ is the hemispheric mean of the quantity $-\partial\overline{\theta}/\partial p$; and f is the Coriolis parameter at 43°N (1.0×10^{-4} s^{-1}), to simplify the calculation (Holopainen and Fortelius, 1987). The term R in Eq. (3) represents all remaining components in the quasi-geostrophic potential vorticity balance, such as horizontal advection by the time-mean flow, diabatic effects and friction. The subscripts "heat" and "vort" indicate feedback forcing of the high-frequency transient eddy heat flux and vorticity flux, respectively. Other variables are commonly used meteorological variables. Following Holopainen and Fortelius (1987) and Shi (2013), the two-dimensional Laplace operator in Eq. (3) is calculated using a spherical harmonics function with T21 truncated.

3. Relationship between the NPSTF and EAJS

Figure 2 shows the March–April–May mean SST gradient and its variance using three different SST datasets. The three datasets consistently show a pronounced large SST gradient between 20°N and 30°N, extending northeastward from eastern Taiwan to the central North Pacific, with a maximum up to 0.8°C (100 km)$^{-1}$. A maximum variance is also located over this region of large SST gradient. Accordingly, the subtropical parallelogram region (22.5°–33°N, 139.5°E–190.5°W) is defined as the key region of the NPSTF (red box in Fig. 2) in this study. The NPSTF index is then defined as the normalized anomalies of the amplitude of the SST gradient over the key region. A higher (lower) NPSTF index indicates a larger (smaller) amplitude of the SST gradient over the key region and a stronger (weaker) NPSTF. Since the index values based on the three datasets are highly correlated (their correlation coefficients exceed the 99% confidence level; Fig. 3), we use the HadISST dataset in the rest of the paper and check the results using the other two datasets, which do not change qualitatively.

Figure 4 shows the regression coefficient of wind speed at 200 hPa onto the NPSTF index in spring. The NPSTF index shows a significant positive relationship with the 200 hPa wind speed around the center of the climatological EAJS in spring, which extends northeastward from East China to Northwest America via the central Pacific. This positive correlation suggests that the EAJS is significantly enhanced when a strong NPSTF is present. Figure 5 shows the regression coefficients of geopotential height and horizontal wind

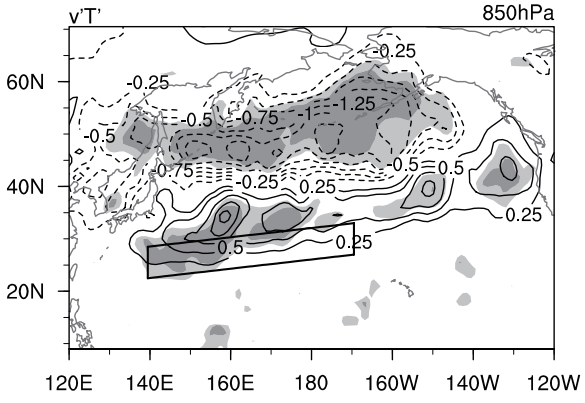

Fig. 7. Regression coefficients (contours) of 850 hPa meridional eddy heat flux [$v'T'$; units: °C (m s^{-1})] onto the NPSTF index in spring. Light and heavy shading represents statistically significant coefficients exceeding the 95% and 99% confidence levels, respectively. The box indicates the key area of the NPSTF.

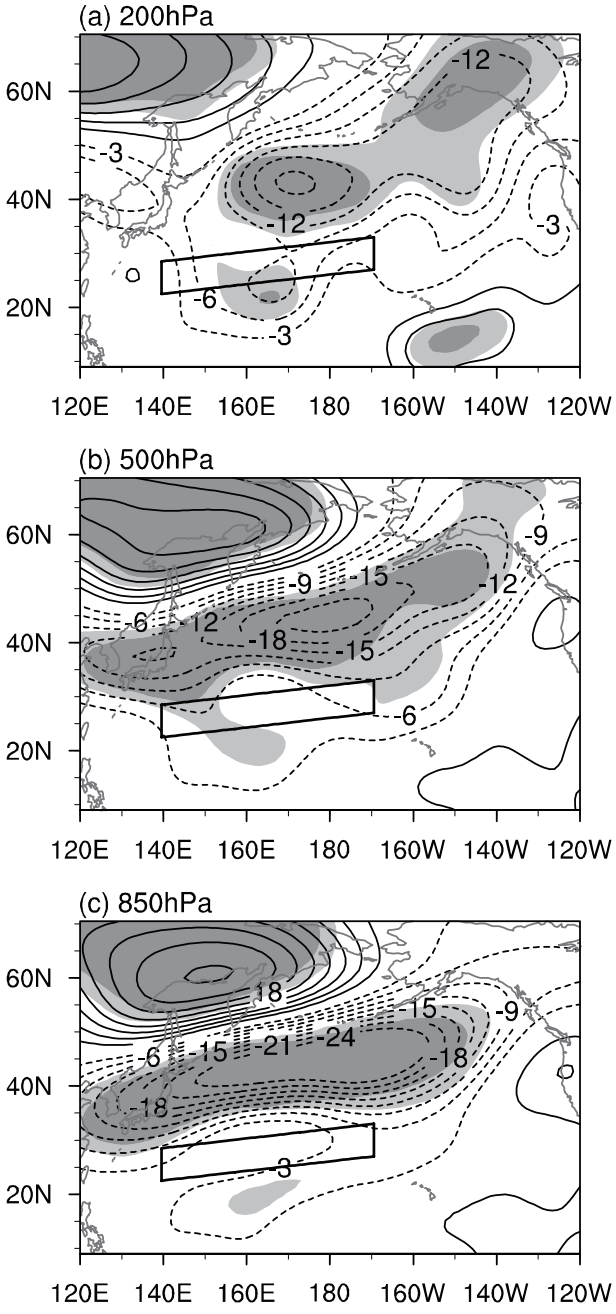

Fig. 8. Regression coefficients (contours) of low-frequency geopotential height due to TEFF (contour interval: 3.0 m^2 s^{-2} d^{-1}) onto the NPSTF index in spring: (a) 200 hPa; (b) 500 hPa; (c) 850 hPa. Light and heavy shading represents statistically significant coefficients exceeding the 95% and 99% confidence levels, respectively. The box indicates the key area of the NPSTF.

upon the NPSTF index. It can be clearly seen that when the NPSTF is developed, the related anomalous geopotential height exhibits an equivalent barotropic structure throughout the troposphere, characterized by a negative geopotential height anomaly over the central North Pacific to the north of the NPSTF (Kobashi et al., 2008) and two positive geopotential height anomalies over Northeast Asia and the central Pacific, respectively. Correspondingly, a significant southwesterly wind anomaly appears over the EAJS core around 30°N, while a northeasterly wind anomaly is found south of the Bering Sea, which is consistent with the changes in the 200 hPa wind (Fig. 4).

4. Possible processes

4.1. *Transient eddy activity*

Figure 6a shows the vertical structure of the regression coefficient of air temperature onto the NPSTF index in spring. A significant anomalous atmospheric warming appears to the south of the front near 25°N, while the opposite is found to the north of the front, resulting in an enhanced atmospheric temperature gradient in the whole troposphere near 30°N (Fig. S2 in ESM). According to Eq. (1), an increase in horizontal temperature gradient can cause a pronounced increase in the atmospheric baroclinicity index (Fig. 6b), which occurs in the low levels (1000 hPa) over the front, near 20°–30°N, and extends up to the upper troposphere (~250 hPa) to the north of the NPSTF. However, the atmospheric baroclinicity is markedly suppressed over the tropics (south of 20°N) and over the middle and high latitudes (north of 45°N).

Increased atmospheric baroclinicity usually induces enhanced synoptic-scale eddy activities (Simmons and Hoskins, 1978). In this study, the intensity of synoptic-scale transient eddy activities is measured by 850 hPa meridional eddy heat flux ($v'T'$) (Blackmon et al., 1977). Figure 7 shows the regression coefficient of 850 hPa meridional eddy heat flux onto the NPSTF index in spring. We can see that changes in the meridional eddy heat flux correspond well to those in the atmospheric baroclinicity index. The enhanced transient eddy activities appear over the NPSTF and to its north, where the atmospheric baroclinicity index is relatively large (Fig. 6b), while the opposite is seen over the middle and high latitudes. Lau and Holopainen (1984) used the framework of a quasi-geostrophic equation to examine the transient eddy forcing effect on time-mean flow. From the solutions of the quasi-geostrophic equation [Eq. (3)] for a simplified system, they

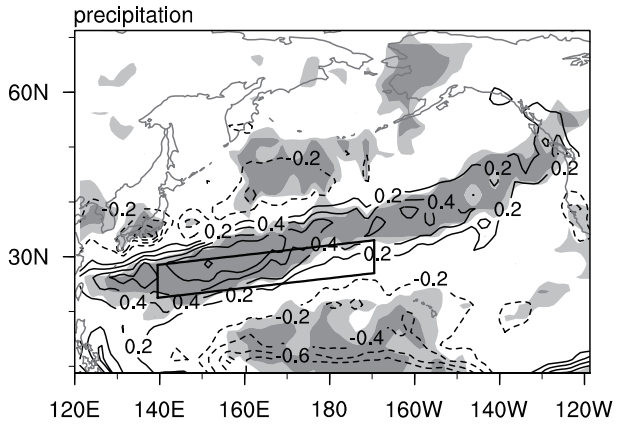

Fig. 9. As in Fig. 7, except for precipitation (units: mm d^{-1}) in spring.

found that enhanced transient eddy activities can trigger an anomalous cyclonic circulation to the north and an anomalous anticyclonic circulation to the south via the anomalous convergence of transient vorticity flux and heat flux (Lau and Holopainen, 1984; Shi, 2013), which was confirmed by numerical simulations (Lau and Holopainen, 1984; Watanabe and Kimoto, 2000). Similarly, as shown in Fig. 8, a significant cyclonic height anomaly appears to the north of the enhanced transient eddy activities and displays a significant equivalent barotropic structure, with its center over the central Pacific and titled eastward with height. Thus, the related westerly wind anomalies over ~30°N benefit an intensified EAJS over the Northeast Pacific (east of ~160°E). Note that TEFF denotes a low-frequency geopotential tendency due to transient eddies. Although the amplitude of TEFF may be small for a single day, it cannot be ignored for a whole season (Shi, 2013).

On the other hand, significantly suppressed transient eddy activities appear south of the Bering Sea (Fig. 7). This may be due to the weakened EAJS caused by the anomalous easterlies north of the cyclonic height anomalies (Ren and Zhang, 2006; Ren et al., 2010). In this scenario, the NPSTF may extend its influence even to mid- and high-latitude regions through anomalous transient eddy activities. As shown in Fig. 8, the anomalous anticyclonic circulation over Northeast Asia is enhanced by TEFF (Fig. 7). Moreover, the anticyclonic height anomalies can contribute to the maintenance of cyclonic height anomalies and further benefits the enhancement of the EAJS over the Northeast Pacific.

As mentioned above, a stronger NPSTF can excite an anomalous cyclonic circulation throughout the troposphere by enhancing the transient eddy activities over the subtropical region; the related westerly wind anomaly on the south side of this anomalous cyclone can enhance the EAJS over the Northeast Pacific (Fig. 4). On the other hand, the enhanced transient activities over the NPSTF act to weaken the transient activities in the middle and high latitudes, which in turn is favorable for the maintenance of the anomalous cyclonic circulation through the TEFF. Therefore, this coupled south–north response of transient eddy activities confirms that the NPSTF can influence the EAJS via changing baroclinicity and transient eddy activities in the free atmosphere. Note that the vertical mixing mechanism is important in the atmospheric adjustment to midlatitude SST fronts in which an increase (decrease) in SST enhances (reduces) the baroclinicity of the near-surface atmosphere and accelerates (decelerates) the surface wind (Wallace et al., 1989; Xie et al., 2002). In our results, the enhanced baroclinicity related to the NPSTF is located over the front in the lower troposphere and over the cold SST side in the upper troposphere. This is consistent with Xie (2004) and Kobashi et al. (2008), who pointed out that the response of baroclinicity to the NPSTF appears different from the prevailing wind adjustment to SST fronts elsewhere, and suggested that some other mechanisms are responsible for the cyclonic circulation along the STF.

4.2. *Atmospheric heat source*

Ding and Liu (2001) suggested that the intensified horizontal air temperature gradient and atmospheric baroclinicity in a cold surge can provide disturbances or mesoscale systems in the frontal zone and further lead to enhanced convective activities. Figure 9 shows the regression coefficient of precipitation onto the NPSTF index in spring. Precipitation is increased near the strong NPSTF, and the associated

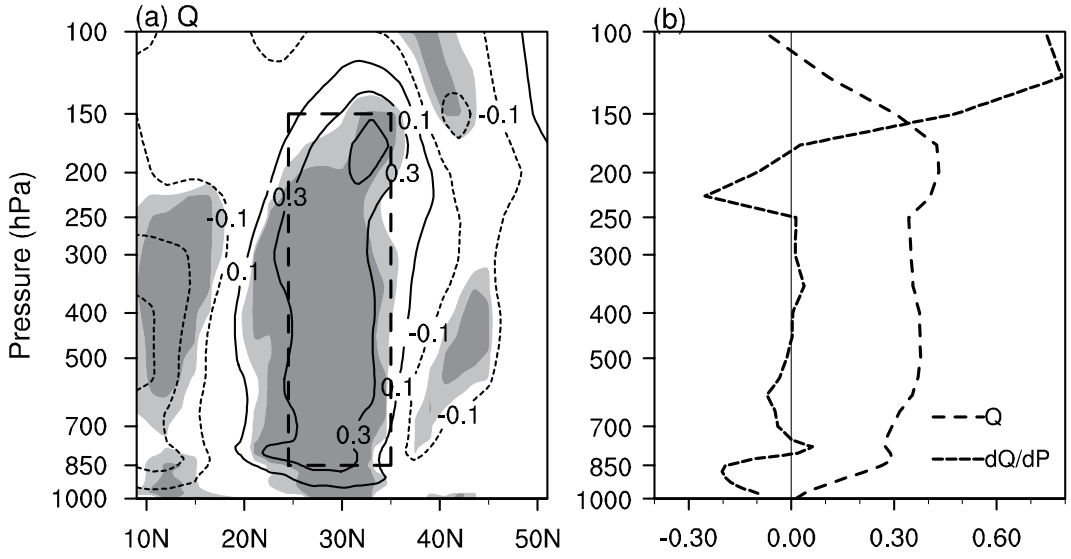

Fig. 10. The (a) latitude–height section of the regression coefficients of the atmospheric heat source (units: W m^{-2}) onto the NPSTF index in spring, and (b) its vertical profile and vertical difference against pressure. Regression coefficients are zonally averaged over 139.5°E–190.5°W in (a) and area-averaged over (24.5°–35.5°N, 139.5°E–90.5°W) in (b). The thick dashed box in (a) indicates the key area of the atmospheric heat source. Light and heavy shading in (a) represents statistically significant coefficients exceeding the 95% and 99% confidence levels, respectively.

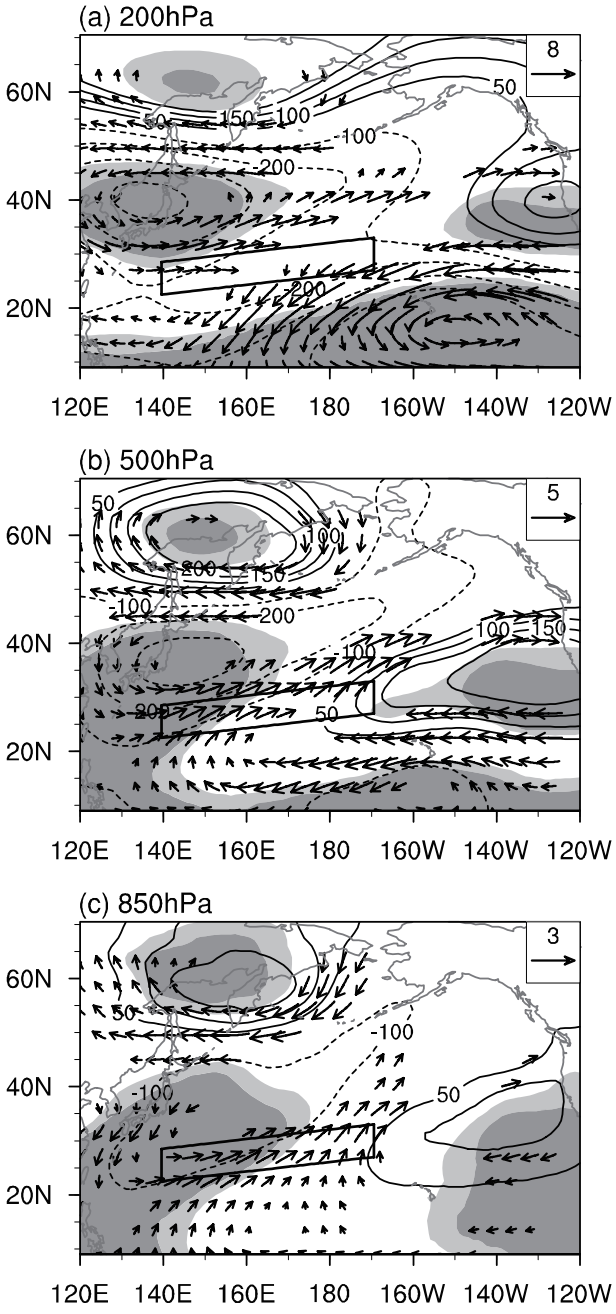

Fig. 11. As in Fig. 5, except for regression coefficients onto the atmospheric heat source index.

condensation latent heating should favor a strong atmospheric heat source. As shown in Fig. 10a, corresponding to the strong NPSTF, a significantly enhanced atmospheric heat source emerges north of the NPSTF throughout the whole troposphere. According to scale analysis and solely taking latent heat into account, Liu et al. (1999) and Wu et al. (1999) simplified the complete form of the vertical vorticity equation to $\beta v \propto \partial Q/\partial z \propto -\partial Q/\partial p$ where v is meridional velocity. Therefore, the atmospheric heat source can trigger anomalous southerly wind ($v > 0$) at the bottom of the maximum heat source ($\partial Q/\partial p < 0$) and anomalous northerly wind ($v < 0$) at the top of the maximum heat source ($\partial Q/\partial p > 0$). Figure 10b displays the vertical profile of the regression coefficient of atmospheric heat source onto the NPSTF index in spring, together with its vertical difference against pressure. We can clearly see that the anomalous maximum center of the heat source is located at 200 hPa and $\partial Q/\partial p$ is almost negative in the troposphere. Therefore, an anomalous heat source associated with the stronger NPSTF index can excite negative $\partial Q/\partial p$ in the troposphere. According to the theory proposed by previous studies (Liu et al., 1999; Wu et al., 1999), negative $\partial Q/\partial p$ can favor the formation of an anomalous cyclonic circulation to its west and an anomalous anticyclonic circulation to its east due to the anomalous southerly wind. To confirm the above results, we define an atmospheric heat source index by vertically integrating the atmospheric heat source from 850 to 150 hPa over 24.5°–35.5°N (box in Fig. 10a). Figure 11 shows the regression coefficients of geopotential height and wind onto the heating index. At different pressure levels, an anomalous cyclonic circulation consistently occurs over the North Pacific and anticyclonic circulation anomalies are found over Northeast Asia and the central Pacific, respectively, which bear a close resemblance with those in Fig. 5 and are consistent with the findings of Liu et al. (1999). Compared to the responses of TEFF (Fig. 8), the main difference is the farther westward location of the anomalous cyclonic circulation. Accordingly, the related significant westerly wind anomalies in the upper troposphere near 30°N act to intensify the component of the EAJS over the Northwest Pacific (west of ~180°). Therefore, increased precipitation due to a strong NPSTF leads to an enhanced atmospheric heat source via condensation latent heating, which may excite an anomalous cyclonic circulation in the upper levels to the west of the source region and subsequently intensifies the EAJS over the Northwest Pacific.

5. Modeling

In light of the above analysis, a strong NPSTF in spring could significantly enhance the 200 hPa wind via enhanced transient eddy activity and an enhanced atmospheric heat source. In this section, five numerical experiments based on CAM5.1 are used to verify the above conclusions.

CAM5.1 has a horizontal resolution of $1.9° \times 2.5°$ (lat $\times$ lon) and a hybrid vertical coordinate with 30 levels, and is forced by the climatological monthly-mean SST during 1986–2005. All experiments are first integrated for five years and meteorological variables on 1 March in the sixth year are used as the initial conditions to run the following three months (March–April–May) with different SST gradients over the North Pacific subtropics. In the control experiment (CTRL), the model is run with the climatological SST. Figure 12 shows the wind speed at 200 hPa in spring from the ERA-Interim observations and CTRL. In CTRL, the 200 hPa wind speed has a maximum over southern Japan and extends northeastward from eastern China to the North Pacific, which is consistent with the observation except for a rela-

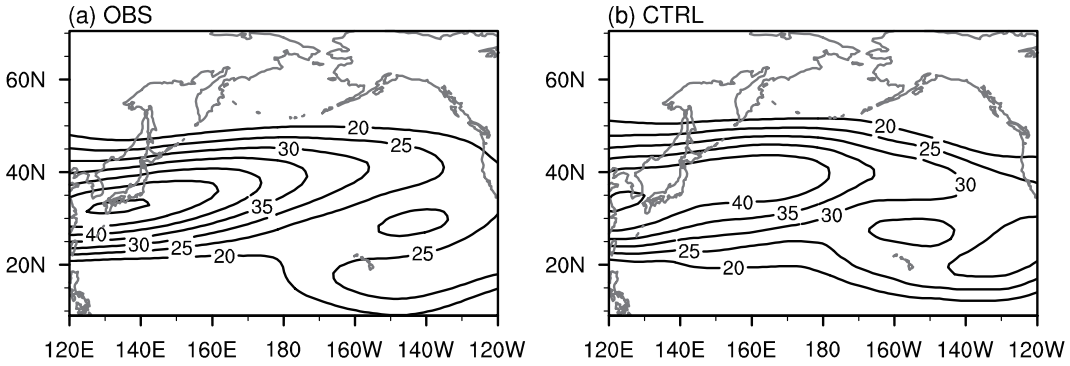

Fig. 12. The (a) observed and (b) CTRL-simulated wind speed (units: m s^{-1}) at 200 hPa in spring.

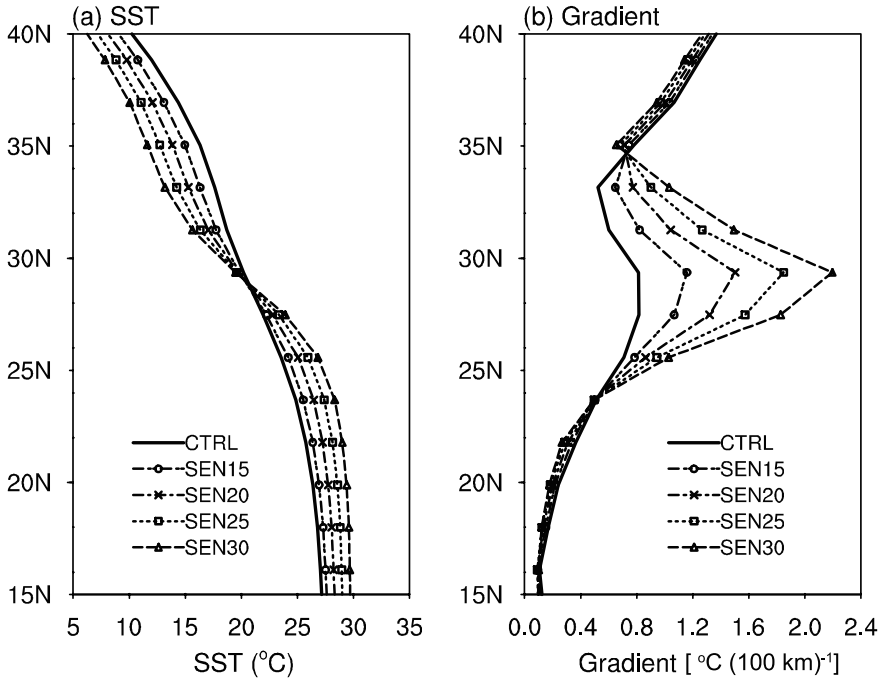

Fig. 13. Variation of (a) zonal-mean SSTs (units: °C) and (b) SST gradients [units: °C (100 km)$^{-1}$] zonally averaged over 139.5°E–190.5°W in the CTRL and sensitivity experiments.

tively weaker maximum center. On the whole, CAM5.1 simulates the atmospheric circulation in spring well (Deng et al., 2014; Deng and Xu, 2015; Zhao et al., 2015).

A set of sensitivity experiments with enhanced SST gradients over the NPSTF region are conducted to investigate the atmospheric responses of the NPSTF. In these sensitivity experiments, the SST gradients over the key area of the NPSTF are artificially amplified by a factor of 1.5 (SEN15), 2.0 (SEN20), 2.5 (SEN25), and 3.0 (SEN30). The SSTs and their gradients, zonally averaged over (139.5°E–190.5°W) in these sensitivity experiments, are shown in Fig. 13.

Figure 14 shows the differences of 200 hPa geopotential height and horizontal wind in spring between the sensitivity experiments and CTRL. For all sensitivity experiments, a negative geopotential height anomaly occurs over the central North Pacific north of the NPSTF, while a positive one is situated over the central Pacific. Correspondingly, a southwesterly wind anomaly appears over the EAJS core around 30°N, which is consistent with our findings based on the observations (section 3). Moreover, amplitudes of geopotential height and wind anomalies are increased with an intensified NPSTF. Thus, these model simulations further confirm that anomalous westerly wind in the upper troposphere is indeed caused by the NPSTF.

6. Conclusions and discussion

This study investigates the relationship between the NPSTF and atmospheric circulation in spring on the interannual timescale. The results show that a strong NPSTF in spring can prominently enhance the EAJS. Both transient eddy activity and the atmospheric heat source play dominant roles in this process. The enhanced atmospheric temperature gradient due to a strong NPSTF increase atmospheric baro-

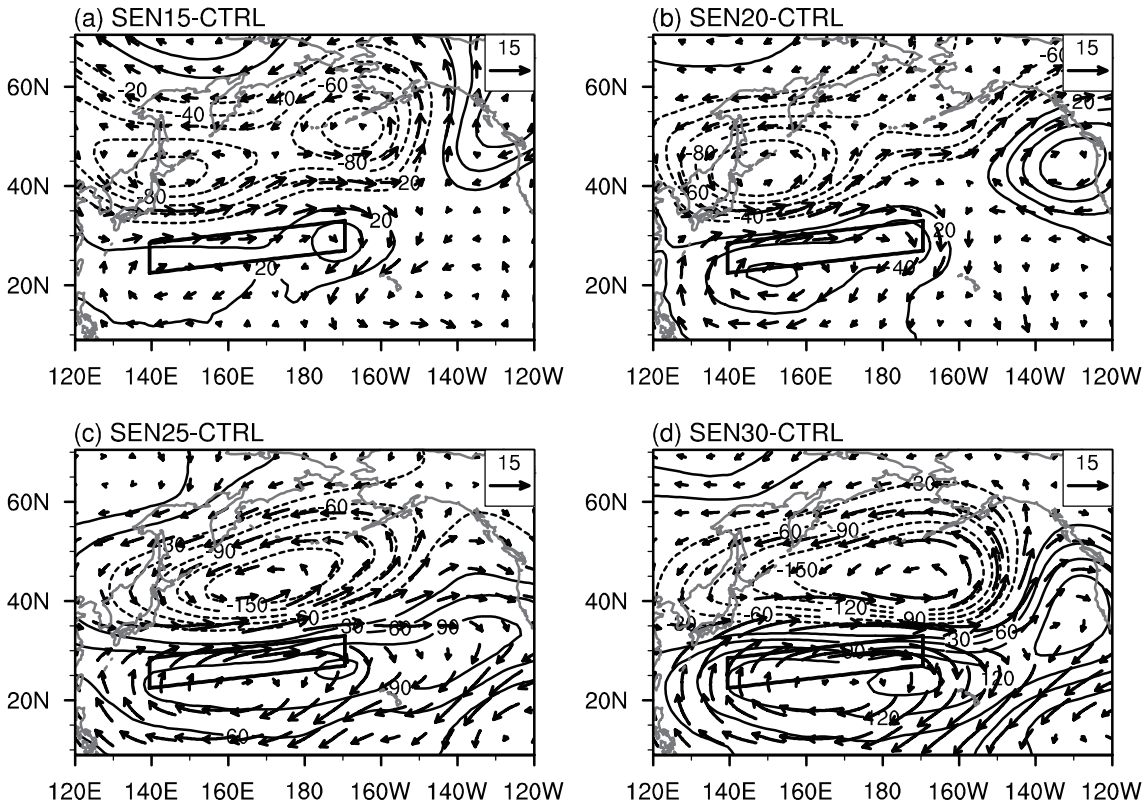

Fig. 14. Differences in geopotential height (contours; units: $m^2\ s^{-2}$) and horizontal wind (vectors; units: $m\ s^{-1}$) at 200 hPa in spring (a) between SEN15 and CTRL, (b) between SEN20 and CTRL, (c) between SEN25 and CTRL, and (d) between SEN30 and CTRL. Contour intervals are 20 $m^2\ s^{-2}$ in (a, b) and 30 $m^2\ s^{-2}$ in (c, d).

clinicity, resulting in an intensification of transient eddy and convection activities. On the one hand, the enhanced transient activities can excite an anomalous cyclonic circulation in the troposphere north of the NPSTF around 40°N; and the related westerly wind anomalies to its south in the upper troposphere can intensify the EAJS over the Northeast Pacific. In addition, the enhanced transient eddy activities in the vicinity of the NPSTF act to suppress the transient eddy activities over the middle and high latitudes. The suppressed transient eddy activities can excite an anomalous anticyclonic circulation to its north, which in turn favors the maintenance of a cyclonic circulation anomaly. On the other hand, an enhanced atmospheric heat source appears over the NPSTF, which is related to increased rainfall. The enhanced heat source can excite an anomalous cyclonic circulation in the troposphere to its west, near 40°N, which induces an enhancement of the EAJS over the Northwest Pacific. The results of a set of numerical experiments further confirm that anomalous westerly wind in the upper troposphere is indeed caused by the NPSTF. Note that as two types of behavior of an unstable atmosphere, the enhanced transient eddy activities and the atmospheric heat source associated with the NPSTF may not be independent. However, their influences on the atmospheric circulation prevail over different regions, suggesting that these two factors may combine to enhance the EAJS—a suggestion that needs further study.

As is well known, ENSO is the most dominant factor in air–sea interaction on the interannual timescale; it governs atmospheric circulation all over the world, especially over the North Pacific and East Asia (Zhang et al., 1999; Zhou et al., 2010). The question therefore naturally arises as to whether ENSO modulates the relationship between the NPSTF and the EAJS. We find that the results presented in this paper do not change (qualitatively) when the ENSO signals are filtered out in advance, as in Gong et al. (2011) (Fig. S3 in ESM). In addition, there are stronger SST fronts in the midlatitudes of the North Pacific (Fig. 1), which also have significant influences on the atmospheric circulation over the North Pacific (Tanimoto et al., 2009; Kwon et al., 2010; Xu et al., 2010b; Xu and Xu, 2015). Thus, we define a midlatitude SST front index based on the normalized SST gradient over (31°–37°N, 140°E–180°) (Qiu, 2000; Wang et al., 2011) and recalculate the correlation between the NPSTF and the EAJS with the midlatitude SST front index filtered out in advanced. Results show that the NPSTF index still has a significant positive relationship with the 200 hPa wind speed around the center of the climatological EAJS (Fig. S4 in ESM), which is consistent with our findings presented in section 3. However, the relationship between the midlatitude SST fronts and the NPSTF over the North Pacific needs further investigation. Moreover, we perform a comparative analysis using NCEP–NCAR reanalysis data (Kalnay et al., 1996). The results are consistent with those using ERA-Interim. As shown in Fig. 15, the zonal winds are enhanced significantly in the whole tropo-

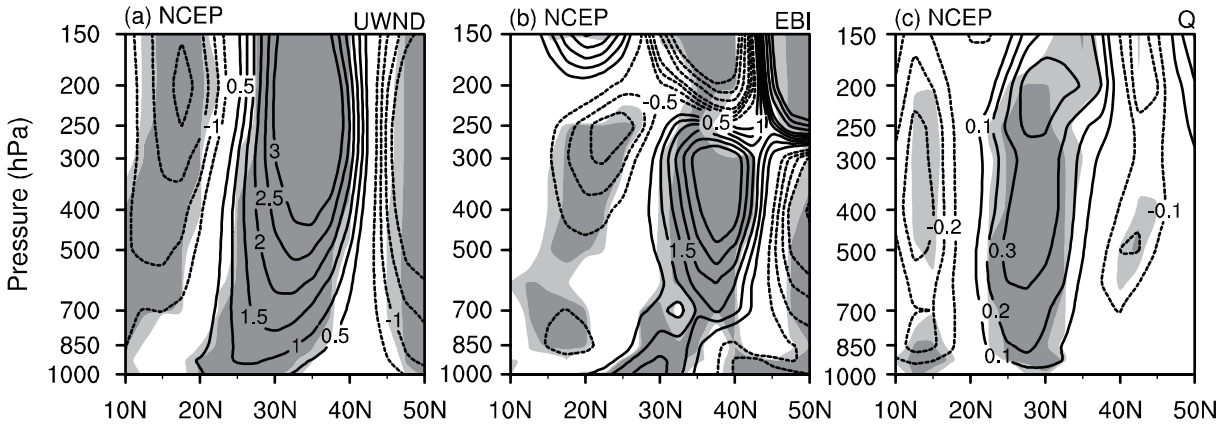

Fig. 15. Latitude–height section of the regression coefficients of (a) zonal wind (contour interval: 0.5 m s^{-1}), (b) atmospheric baroclinicity index (contour interval: 0.5×10^{-2} d^{-1}), and (c) atmospheric heat source (contour interval: 0.1 W m^{-2}), onto the NPSTF index in spring. Zonal wind, atmospheric baroclinicity and the atmospheric heat source are zonally averaged over 140°E–190°W for the NCEP reanalysis dataset. Light and heavy shading represents statistically significant coefficients exceeding the 95% and 99% confidence levels, respectively.

sphere around 30°N due to a strong NPSTF, accompanying the intensification of atmospheric baroclinicity and the atmospheric heat source.

Qiu and Chen (2010) found that increased eddy kinetic energy along the North Pacific subtropical countercurrent (STCC), whose upward-titling thermocline is also called the NPSTF, is due to the enhanced baroclinic instability associated with the large vertical shear in the STCC background flow. Although they proposed that the interannual variation of the STCC is driven by a western Pacific pattern through Ekman transport convergence, they also suggested that there is positive feedback in the coupled air–sea interaction over the North Pacific in spring, which may be one reason why the NPSTF is most pronounced in spring. Our numerical results just confirm the significant influence of the NPSTF on the general circulation over the western Pacific, complementary to Qiu and Chen (2010). In addition to the interannual variability, the NPSTF and EAJS also exhibit significant intraseasonal variability (Kuang et al., 2007; Xie et al., 2015); further study is needed to investigate their relationship on this timescale.

Acknowledgements. We are grateful to the two anonymous reviewers and editors for their constructive comments. This work was jointly supported by the Ministry of Science and Technology of China, through the National Basic Research Program of China (Grant No. 2012CB955602); the National Natural Science Foundation of China (Grant Nos. 41575077, 41490643 and 41275094); and a project funded by the PAPD (Priority Academic Program Development of Jiangsu Higher Education Institutions). Leying ZHANG was supported by the Innovation Project for Graduate Student of Jiangsu Province (Grant No. KYLX15-0860).

Electronic supplementary material: Supplementary material is available in the online version of this article at http://dx.doi.org/10.1007/s00376-016-6026-x.

REFERENCES

Awan, J. A., and D. H. Bae, 2016: Features and interdecadal variability of droughts in the homogeneous rainfall zones over the East Asian monsoon region. *Int. J. Climatol.*, **36**, 1943–1953, doi: 10.1002/joc.4471.

Blackmon, M. L., J. M. Wallace, N. C. Lau, and S. L. Mullen, 1977: An observational study of the Northern Hemisphere wintertime circulation. *J. Atmos. Sci.*, **34**, 1040–1053, doi: 10.1175/1520-0469(1977)034<1040:AOSOTN>2.0.CO;2.

Brayshaw, D. J., B. Hoskins, and M. Blackburn, 2008: The storm-track response to idealized SST perturbations in an aquaplanet GCM. *J. Atmos. Sci.*, **65**, 2842–2860.

Charney, J. G., 1947: The dynamics of long waves in a baroclinic westerly current. *J. Meteor. Soc.*, **4**, 136–162.

Dee, D. P., and Coauthors, 2011: The ERA-interim reanalysis: configuration and performance of the data assimilation system. *Quart. J. Roy. Meteor. Soc.*, **137**, 553–597.

Deng, J. C., and H. M. Xu, 2015: Atmospheric responses to idealized urban land surface forcing in eastern China during the boreal spring. *J. Geophys. Res.*, **120**, 10 022–10 039.

Deng, J. C., H. M. Xu, H. Y. Ma, and Z. H. Jiang, 2014: Numerical study of the effect of anthropogenic aerosols on spring persistent rain over Eastern China. *Journal of Meteorological Research*, **28**, 341–353.

Ding, Y. H., 1989: *Diagnostic Analysis Method in Weather Dynamics*. Science Press, 293 pp. (in Chinese)

Ding, Y. H., and Y. J. Liu, 2001: Onset and the evolution of the summer monsoon over the South China Sea during SCSMEX field experiment in 1998. *J. Meteor. Soc. Japan Ser. II*, **79**(S), 255–276.

Eady, E. T., 1949: Long waves and cyclone waves. *Tellus*, **1**, 33–52.

Gong, D. Y., and C. H. Ho, 2003: Arctic oscillation signals in the East Asian summer monsoon. *J. Geophys. Res.*, **108**(D2), 4066, doi: 10.1029/2002JD002193.

Gong, D. Y., J. Yang, S. J. Kim, Y. Q. Gao, D. Guo, T. J. Zhou, and M. Hu. 2011: Spring Arctic Oscillation–East Asian summer monsoon connection through circulation changes over the western North Pacific. *Climate Dyn.*, **37**, 2199–2216.

Hayes, S. P., M. J. McPhaden, and J. M. Wallace, 1989: The influence of sea-surface temperature on surface wind in the eastern Equatorial Pacific: Weekly to monthly variability. *J. Climate*, **2**, 1500–1506.

Holopainen, E., and C. Fortelius, 1987: High-frequency transient eddies and blocking. *J. Atmos. Sci*., **44**, 1632–1645.

Hoskins, B. J., and P. J. Valdes, 1990: On the existence of storm-tracks. *J. Atmos. Sci*., **47**, 1854–1864.

James, I. N., 1987: Suppression of baroclinic instability in horizontally sheared flows. *J. Atmos. Sci*., **44**, 3710–3720.

Kalnay, E., and Coauthors, 1996: The NCEP/NCAR 40-year reanalysis project. *Bull. Amer. Meteor. Soc*., **77**, 437–470.

Kobashi, F., and A. Kubokawa, 2012: Review on North Pacific subtropical countercurrents and subtropical fronts: Role of mode waters in ocean circulation and climate. *J. Oceanogr.*, **68**, 21–43.

Kobashi, F., S. P. Xie, N. Iwasaka, and T. T. Sakamoto, 2008: Deep atmospheric response to the North Pacific oceanic subtropical front in spring. *J. Climate*, **21**, 5960–5975.

Kuang, X. Y., Y. C. Zhang, and J. Liu, 2007: Seasonal variations of the East Asian subtropical westerly jet and the thermal mechanism. *Acta Meteorologica Sinica*, **21**, 192–203.

Kubokawa, A., 1995: Stationary Rossby waves and shocks on the Sverdrup coordinate. *J. Oceanogr.*, **51**, 207–224.

Kubokawa, A., 1997: A two-level model of subtropical gyre and subtropical countercurrent. *J. Oceanogr.*, **53**, 231–244.

Kubokawa, A., 1999: Ventilated thermocline strongly affected by a deep mixed layer: A theory for subtropical countercurrent. *J. Phys. Oceanogr*., **29**, 1314–1333.

Kuwano-Yoshida, A., S. Minobe, and S. P. Xie, 2010: Precipitation response to the Gulf Stream in an atmospheric GCM. *J. Climate*, **23**, 3676–3698.

Kwon, Y.-O., M. A. Alexander, N. A. Bond, C. Frankignoul, H. Nakamura, B. Qiu, and L. Thompson, 2010: Role of the Gulf Stream and Kuroshio-Oyashio systems in large-scale atmosphere-ocean interaction: A review. *J. Climate*, **23**, 3249–3281.

Lau, N. C., and E. O. Holopainen, 1984: Transient eddy forcing of the time-mean flow as identified by geopotential tendencies. *J. Atmos. Sci*., **41**, 313–328.

Lau, N. C., and M. J. Nath, 1991: Variability of the baroclinic and barotropic transient eddy forcing associated with monthly changes in the midlatitude storm tracks. *J. Atmos. Sci*., **48**, 2589–2613.

Liang, X. Z., and W. C. Wang, 1998: Associations between China monsoon rainfall and tropospheric jets. *Quart. J. Roy. Meteor. Soc*., **124**, 2597–2623.

Lindzen, R. S., and B. Farrell, 1980: A simple approximate result for the maximum growth rate of baroclinic instabilities. *J. Atmos. Sci*., **37**, 1648–1654.

Lindzen, R. S., and R. S. Nigam, 1987: On the role of sea surface temperature gradients in forcing low-level winds and convergence in the tropics. *J. Atmos. Sci*., **44**, 2418–2436.

Liu, Y. M., G. X. Wu, H. Liu, P. Liu, 1999: The effect of spatially nonuniform heating on the formation and variation of subtropical high Part III: Condensation heating and south Asian high and western Pacific subtropical high. *Acta Meteorologica Sinica*, **57**, 525–538. (in Chinese)

Lu, R. Y., Z. D. Lin, and Y. C. Zhang, 2013: Variability of the East Asian upper-tropospheric jet in summer and its impacts on the East Asian monsoon. *Chinese J. Atmos. Sci.*, **37**, 331–340. (in Chinese)

Minobe, S., A. Kuwano-Yoshida, N. Komori, S. P. Xie, and R. J. Small, 2008: Influence of the Gulf Stream on the troposphere. *Nature*, **452**, 206–209.

Nakamura, H., and T. Sampe, 2002: Trapping of synoptic-scale disturbances into the North-Pacific subtropical jet core in midwinter. *Geophys. Res. Lett*., **29**, 8-1–8-4, doi: 10.1029/2002GL015535.

Nakamura, M., and S. Yamane, 2010: Dominant anomaly patterns in the near-surface baroclinicity and accompanying anomalies in the atmosphere and oceans. Part II: North Pacific basin. *J. Climate*, **23**, 6445–6467.

Nakamura, M., and T. Miyama, 2014: Impacts of the Oyashio temperature front on the regional climate. *J. Climate*, **27**, 7861–7873.

Ogawa, F., H. Nakamura, K. Nishii, T. Miyasaka, and A. Kuwano-Yoshida, 2012: Dependence of the climatological axial latitudes of the tropospheric westerlies and storm tracks on the latitude of an extratropical oceanic front. *Geophys. Res. Lett*., **39**, doi: 10.1029/2011GL049922.

O'Reilly, C. H., and A. Czaja, 2015: The response of the Pacific storm track and atmospheric circulation to Kuroshio extension variability. *Quart. J. Roy. Meteor. Soc*., **141**, 52–66, doi: 10.1002/qj.2334.

Qiu, B., 2000: Interannual variability of the Kuroshio extension system and its impact on the wintertime SST field. *J. Phys. Oceanogr*., **30**, 1486–1502.

Qiu, B., and S. M. Chen, 2010: Interannual variability of the North Pacific subtropical countercurrent and its associated mesoscale eddy field. *J. Phys. Oceanogr*., **40**, 213–225.

Rayner, N. A., D. E. Parker, E. B. Horton., C. K. Folland, L. V. Alexander, D. P. Rowell, E. C. Kent, and A. Kaplan, 2003: Global analyses of sea surface temperature, sea ice, and night marine air temperature since the late Nineteenth Century. *J. Geophys. Res.*, **108**(D14), doi: 10.1029/2002JD002670.

Ren, X. J., and Y. C. Zhang, 2006: Association of winter western Pacific jet stream anomalies at 200 hPa with ocean surface heating and atmospheric transient eddies. *Acta Meteorologica Sinica*, **65**, 550–560. (in Chinese)

Ren, X. J., X. Q. Yang, and C. J. Chu, 2010: Seasonal variations of the synoptic-scale transient eddy activity and polar front jet over East Asia. *J. Climate*, **23**, 3222–3233.

Reynolds, R. W., and D. B. Chelton, 2010: Comparisons of daily sea surface temperature analyses for 2007–08. *J. Climate*, **23**, 3545–3562.

Roden, G. I., 1975: On North Pacific temperature, salinity, sound velocity and density fronts and their relation to the wind and energy flux fields. *J. Phys. Oceanogr*., **5**, 557–571.

Sampe, T., H. Nakamura, A. Goto, and W. Ohfuchi, 2010: Significance of a midlatitude SST frontal zone in the formation of a storm track and an eddy-driven westerly jet. *J. Climate*, **23**, 1793–1814.

Shi, N., 2013: Role of high-frequency transient eddy feedback forcing in the evolution of East Asia-Pacific events. *Chinese J. Atmos. Sci.*, **37**, 1187–1198. (in Chinese)

Simmons, A. J., B. J. Hoskins, 1978: The life cycles of some nonlinear baroclinic waves. *J. Atmos. Sci*., **35**, 441–432.

Small, R. J., S. P. Xie, and Y. Q. Wang, 2003: Numerical simulation of atmospheric response to Pacific tropical instability waves. *J. Climate*, **16**, 3723–3741.

Tanimoto, Y., S. P. Xie., K. H. Kai, H. Okajima, H. Tokinaga, T. Murayama, M. Nonaka, and H. Nakamura, 2009: Observations of marine atmospheric boundary layer transitions across

the summer Kuroshio extension. *J. Climate*, **22**, 1360–1374.

Tokinaga, H., Y. Tanimoto, S. P. Xie, T. Sampe, H. Tomita, and H. Ichikawa, 2009: Ocean frontal effects on the vertical development of clouds over the western North Pacific: *In situ* and satellite observations. *J. Climate*, **22**, 4241–4260.

Wallace, J. M., T. P. Mitchell, and C. Deser, 1989: The influence of sea-surface temperature on surface wind in the eastern equatorial Pacific: Seasonal and interannual variability. *J. Climate*, **2**, 1492–1499.

Wang, N., and Y. C. Zhang, 2015: Connections between the Eurasian teleconnection and concurrent variation of upper-level jets over East Asia. *Adv. Atmos. Sci*., **32**, 336–348, doi: 10.1007/s00376-014-4088-1.

Wang, X. D., Z. Zhong, L. L. Qi, and H. H. Yuan. 2011: Response of atmospheric circulation to SST anomalies of Kuroshio extension in winter. *Journal of PLA University of Science and Technology (Natural Science Edition)*, **12**, 541–547. (in Chinese)

Watanabe, M., 2004: Asian jet waveguide and a downstream extension of the North Atlantic oscillation. *J. Climate*, **17**, 4674–4691.

Watanabe, M, and M. Kimoto, 2000: Atmosphere-ocean thermal coupling in the North Atlantic: A positive feedback. *Quart. J. Roy. Meteor. Soc*., **126**, 3343–3369.

Wu, G. X., Y. M. Liu, and P. Liu, 1999: The effect of spatially nonuniform heating on the formation and variation of subtropical high I: Scale analysis. *Acta Meteorologica Sinica*, **57**, 257–263. (in Chinese)

Xie, S. P., J. Hafner, Y. Tanimoto, W. T. Liu, H. Tokinaga, and H. M. Xu, 2002: Bathymetric effect on the winter sea surface temperature and climate of the Yellow and East China Seas. *Geophys. Res. Lett*., **29**, 2228, doi: 10.1029/2002GL015884.

Xie, S. P., 2004: Satellite observations of cool ocean-atmosphere interaction. *Bull. Amer. Meteor. Soc*., **85**, 195–208.

Xie, Z. Q., Y. Du, and S. Yang, 2015: Zonal Extension and Retraction of the subtropical westerly jet stream and evolution of precipitation over East Asia and the Western Pacific. *J. Climate*, **28**, 6783–6798.

Xu, H. M., L. W. Wang, and J. H. He, 2008: Observed oceanic feedback to the atmosphere over the Kuroshio Extension during spring time and its possible mechanism. *Chin. Sci. Bull.*, **53**, 1905–1912.

Xu, H. M., H. Tokinaga, and S. P. Xie, 2010a: Atmospheric effects of the Kuroshio large meander during 2004-05. *J. Climate*, **23**, 4704–4715.

Xu, H. M., M. M. Xu, S. P. Xie, and Y. Q. Wang, 2011: Deep atmospheric response to the spring Kuroshio over the East China Sea. *J. Climate*, **24**, 4959–4972.

Xu, M. M., and H. M. Xu, 2015: Atmospheric responses to Kuroshio SST front in the East China Sea under different prevailing winds in winter and spring. *J. Climate*, **28**, 3191–3211.

Xu, M. M., H. M. Xu, and S. X. Zhu, 2010b: Ocean-to-atmosphere forcing in the vicinity of the sea surface temperature front in East China Sea during spring time and its possible mechanisms. *Chinese J. Atmos. Sci.*, **34**, 1071–1087. (in Chinese)

Yanai, M., S. Esbensen, and J. H. Chu, 1973: Determination of bulk properties of tropical cloud clusters from large-scale heat and moisture budgets. *J. Atmos. Sci*., **30**, 611–627.

Ye, D. Z., S. Y. Tao, and M. C. Li, 1958: The abrupt change of circulation over northern hemisphere during June and October. *Acta Meteorologica Sinica*, **29**, 249–263. (in Chinese)

Yoshida, K., and T. Kidokoro, 1967a: A subtropical countercurrent in the North Pacific-an eastward flow near the subtropical convergence. *J. Oceanogr. Soc. Japan*, **23**, 88–91.

Yoshida, K., and T. Kidokoro, 1967b: A subtropical countercurrent (II)—A prediction of eastward flows at lower subtropical latitudes. *J. Oceanogr. Soc. Japan*, **23**, 231–236.

Zhang, R. H., A. Sumi, and M. Kimoto, 1999: A diagnostic study of the impact of EL Niño on the precipitation in China. *Adv. Atmos. Sci*., **16**, 229–241, doi: 10.1007/BF02973084.

Zhang, Y. C., D. Q. Wang, and X. J. Ren, 2008: Seasonal variation of the meridional wind in the temperate jet stream and its relationship to the Asian monsoon. *Acta Meteor. Sinica*, **66**, 446–454.

Zhao, X., H. M. Xu, M. M. Xu, and J. C. Deng, 2015: The Spring atmospheric heat source over the East China Sea Kuroshio area and its impact on precipitation in Eastern China. *Acta Meteor. Sinica*, **73**, 263–275. (in Chinese)

Zhou, L. T., C. Y. Tam, W. Zhou, and J. C. L. Chan, 2010: Influence of South China Sea SST and the ENSO on winter rainfall over South China. *Adv. Atmos. Sci*., **27**, 832–844, doi: 10.1007/s00376-009-9102-7.